Natural Hazards
and Earth System
Sciences
Discussions

Tsunami fragility curve using field data and numerical simulation of the 2015 tsunami in Coquimbo, Chile

Rafael Aránguiz[1,2], Luisa Urra[3], Ryo Okuwaki[4], Yuji Yagi[5]

[1]Department of Civil Engineering, Universidad Católica de la Santísima Concepción
5   [2]National Research Center for Integrated Natural Disaster Management CONICYT/FONDAP/1511007 (CIGIDEN)
[3]Laboratory of Remote Sensing and Geoinformatics for Disaster Management, International Research Institute of Disaster Science, Tohoku University, Japan
[4]Graduate School of Life and Environmental Sciences, University of Tsukuba, Japan
[5]Faculty of Life and Environmental Sciences, University of Tsukuba, Japan

10   *Correspondence to*: Rafael Aránguiz (raranguiz@ucsc.cl)

Abstract. The last earthquake which affected Coquimbo city took place in September 2015, with localized damage observed in low areas of the city. In addition, another seismic gap north of the 2015 earthquake rupture area has been identified; therefore, a significant earthquake and tsunami could occur in the near future. The present paper develops the tsunami fragility curve for the city of Coquimbo based on field survey data and tsunami numerical simulations. The inundation depth of the 2015 Chile
15   tsunami in Coquimbo was estimated by means of numerical simulation with the NEOWAVE model and 5 nested grids with a maximum grid resolution of 10 m. The fragility curve exhibited behavior similar to that of other curves in plain areas in Japan, where low damage was observed at relatively high inundation depths. The new fragility curve was used to estimate the damage by possible future tsunamis in the area. The damage assessment showed that ~50% of the structures in the lower area of Coquimbo have a high probability of damage in case of a tsunami generated off the coast of the study area if the city is rebuilt
20   with the same type of structures.

1 Introduction

On 16 September 2015 a Mw 8.3 earthquake took place off the coast of the Coquimbo Region (USGS: http://earthquake.usgs.gov/earthquakes/eventpage/us20003k7a#executive). The earthquake generated a tsunami that inundated low areas of the city of Coquimbo, with runup reaching up to 6.4 m and a penetration distance of up to 700 m (Aránguiz et al.,
25   2016; Contreras-López et al., 2016), resulting in reports of significant damage to houses and public infrastructure (Contreras-López et al., 2016). This earthquake filled the seismic gap that had existed since at least the last significant earthquake along the Coquimbo-Illapel seismic region in 1943 (Melgar et al., 2016; Ye et al. 2016) . However, the region just north of the 2015 rupture area has not experienced significant seismic activity since the 1922 Mw 8.3 event (Melgar et al., 2016; Ye et al., 2016). Thus, it is recommended that reconstruction plans and new tsunami mitigation measures consider potential impacts due to
30   possible future tsunamis generated north of the 2015 earthquake rupture zone.

With regard to the assessment of structural damage within the exposed area against potential tsunami hazard, two different approaches were identified. On one hand, damage can be estimated deterministically based on the forces acting on a single structure (Nandasena et al. 2012; Nistor et al. 2009; Shimozono & Sato, 2016; Wei et al., 2015). However, this analysis could be extremely time consuming and impractical for a whole city due to the high-resolution numerical simulations (~2 m) that

5   are required. On the other hand, the assessment of structural damage could be done probabilistically by means of fragility curves (Koshimura et al. 2009; Koshimura et al., 2009(1); Suppasri et al, 2011). Tsunami fragility curves represent the probability of damage to structures in relation to the hydrodynamic features of a tsunami such as the flow depth, current velocity and hydrodynamic force (Koshimura et al. 2009). However, a fully probabilistic approach may use a wide range of possible scenarios, thus both hazard assessment and damage assessment are probabilistic (Park et al., 2017). Empirical tsunami

10   fragility curves were obtained for Banda Aceh in Indonesia (Koshimura et al. 2009) and Thailand (Suppasri et al., 2011) after the 2004 Indian Ocean Tsunami. The same methodology was applied to areas affected by the 2009 Samoa tsunami (Gokon et al., 2014). In a similar manner, this method was applied in Japan after the 2011 Great East Japan tsunami, allowing several fragility curves that considered several damage levels and different building materials to be obtained (Suppasri et al., 2013). After the 2010 Chile tsunami, Mas et al. (2012) developed the first tsunami fragility curve in Chile for masonry and mixed

15   structures in Dichato. Tsunami fragility curves are obtained for a given area under a given scenario; therefore, they may not be applicable when changing the areas of interest since the tsunami characteristics and building materials may differ (Koshimura et al. 2009; Suppasri et al., 2011). In fact, buildings along the Sanriku ria coast in Japan experienced greater damage than structures located in plain areas in Sendai (Suppasri et al., 2013; Suppasri, Mas, et al., 2012). Subsequently, the Coquimbo area provides a good opportunity to develop a fragility curve and assess potential tsunami impact since the tsunami

20   in 2015 did not damage all structures and some of them have been repaired or rebuilt in the same places. The present research develops an empirical fragility curve for the Coquimbo area using field survey data and numerical simulation of the 2015 Chile tsunami. In addition, we estimate the probability of structural damage for a deterministic tsunami scenario using the Coquimbo fragility curve.

2 Study Area

25   The city of Coquimbo is located on the southern shore of Coquimbo Bay (29.96°S). The Coquimbo area was mentioned by the conquistadors as a good place for a port and the location became important due to the natural protection it offered against south-west swell waves, which provided good conditions for its use as a port starting in the XIX century. Coquimbo Bay is open to the northwest and is characterized by a lowland topography with a long, flat, sandy beach (Aránguiz et al., 2016). Like all coastal cities in Chile, Coquimbo is located over the subduction zone of the Nazca Plate beneath the South American plate

30   (18°- 44°S). The convergence rate of the plates is 68 mm/year along the Chile subduction zone and large seismic events take place every 10 years on average (Métois et al. 2016). In fact, 3 events over magnitude 8.0 have taken place in the last 6 years, namely the 2010 Maule (34-38°S) , the 2014 Iquique (19-20°S) and the 2015 Illapel (30-32°S) earthquakes.

Natural Hazards
and Earth System
Sciences
Discussions

Figure 1 shows the seismic events recorded in the Coquimbo area. The oldest record of a tsunami is from the 1730 event. This earthquake generated a destructive tsunami that destroyed Valparaiso and Concepción and flooded low areas in Japan (Cisternas et al., 2011). The tsunami destroyed several ranches on the shore of Coquimbo (Soloviev & Go, 1975). Although the 1880 and 1943 earthquakes are considered to be similar in size (Nishenko, 1985), it is observed that the behavior of the

5   tsunamis generated by these events seem to be different. While the former generated large columns of water that resulted in the anchor chain of a ship snapping in Coquimbo (Soloviev & Go, 1975) and a deep submarine cable breaking off the coast of the Limarí River (Lomnitz, 2004), the latter generated a minor tsunami that damaged fishing boats in Los Vilos and raised the water level by 80 cm in Valparaiso (Soloviev & Go, 1975), while no tsunami was reported in Coquimbo. Conversely, the 2015 tsunami reached up to 4.75 m at the Coquimbo tide gauge, with a runup of 6.4 m (Aránguiz et al., 2016; Contreras-López

10   et al., 2016). Moreover, a maximum tsunami amplitude of 2 m was observed at the Valparaiso tide gauge (Aránguiz et al., 2016). The main reason behind this is that the 1943 event broke the deepest portion of the subduction interface, while the 2015 event had a shallower rupture area and larger magnitude (Fuentes et al., 2016; Okuwaki et al., 2016), resulting in a larger initial tsunami amplitude (Aránguiz et al., 2016).

The largest tsunami ever recorded in Coquimbo took place in 1922. The tsunami arrived in Coquimbo two hours after the

15   earthquake and three large waves were observed, the third of which was the largest, with a maximum tsunami height of 7 m above mean sea level and an inland penetration of 2 km. The part of the city located on the southern shore of Coquimbo Bay was totally destroyed due to both the water and the tsunami debris (Soloviev & Go, 1975). In a similar manner, the tsunami reached up to 9 m at Chañaral and 6-7m at Caldera. The tsunami was also observed in Japan, with maximum amplitudes ranging from 60 to 70 cm (Soloviev & Go, 1975), which is similar to the amplitudes of the 2015 event (80 cm), but larger than

20   those of the 1943 event with 10-25 cm (Beck et al., 1998). Another significant event was the 1849 earthquake, which generated a localized tsunami that mainly affected Coquimbo. The tsunami arrived 10 to 30 min after the earthquake, penetrated 300 m horizontally and rose 5 m above the high tide mark (Soloviev & Go, 1975).

3 Development of the fragility curve

The development of the fragility functions in the present work required three main steps: first, data collection of building

25   damage levels in the Coquimbo area as well as tsunami inundation heights for numerical modeling validation; second, selection of a rupture model of the 2015 earthquake and validation of the tsunami inundation heights for estimation of tsunami inundation depth; and third, GIS analysis and statistical analysis for correlation between damage level and simulated tsunami inundation depth.

3.1 Building damage and tsunami inundation data

30   Soon after the 2015 event, a team surveyed the affected area and collected more than 40 inundation height, flow depth and tsunami runup measurements in the Coquimbo inundation area. The field measurements followed established post-tsunami

survey procedures (Dengler et al., 2003; Dominey-Howes et al., 2012; Synolakis & Okal, 2005) and were corrected for tide level at the time of maximum inundation. At the same time, 585 structures within the inundation area were identified and classified as mixed structures made of wood and masonry (568), reinforced concrete buildings of eight or more stories (4) and very light structures that did not meet minimal building standards (13). The present analysis considered the mixed structures

5   only; therefore, the reinforced concrete and light structures were removed from the fragility curve analysis. Figure 2 shows typical mixed structures and marks of flow depth surveyed in Coquimbo immediately after the 2015 tsunami. Figures 2a and b show masonry houses that were not damaged by the tsunami despite flow depths that ranged from 1.5 to 2 m. Meanwhile, Figures 2c and d show houses with moderate to major damage, possibly to be used after major repairs. As a matter of fact, the house in Figure 2c was being repaired at the time of the field survey and the gray wall in the corner was built a few days earlier.

10   Meanwhile, the house in Figure 2d was abandoned, since all interior walls, windows, doors and the roof were completely damaged and major repairs and retrofitting will be needed. Even though the damage to structure could be due to earthquake and tsunami, it was observed that the damage due to the earthquake was limited (Candia et al., 2017) and the most affected structures were made of adobe (Fernández et al., 2017). Therefore, the present work considered that the damage on flooded structures was only due to the tsunami.

15   Due to the small amount of inundated structures (568), two damage levels were defined; thus, it was possible to obtain one fragility curve. The first level, called "surviving," included structures with no damage or minor to major damage, which correspond to levels 1, 2 and 3 given by Suppasri et al. (2013). These damage levels imply that there is slight to severe damage to non-structural components; therefore, it is possible to use the structures after moderate to major repairs. The other damage level, called "destroyed," included damage levels 4 to 6 according to Suppasri et al. (2013), i.e., structures that experienced

20   severe damage to walls or columns or that had completely collapsed.

Previous works carried out damage inspections using satellite images and field surveys (Koshimura et al., 2009; Mas et al., 2012; Suppasri et al., 2011). However, the satellite image method assumes that buildings with intact roofs are "not destroyed" or "surviving" (Suppasri et al., 2011), but severe damage to columns or interior walls may not be observed (Mas et al., 2012), as in the case of the houses shown in Figures 2c and d. Therefore, the present work employed damage detection based on field

25   surveys only. Figure 3a shows the surveyed buildings and the damage level assigned to the 568 mixed structures. The four reinforced concrete buildings (R.C.) and the 13 light structures (L.S.) that did not meet minimal building standards are also included in the figure. Figure 3b shows the inundation height measurements recorded during the field survey. It is observed that the maximum inundation height was reached in the corner, where the coastal road and the railway converge. Most of the damaged structures were identified at that location as well.

30   **3.2 Tsunami inundation depth**

The tsunami inundation depth was estimated as the difference between tsunami inundation height and ground elevation. Therefore, the tsunami heights were obtained from tsunami numerical simulation of the 2015 event. We tested four available finite fault models, namely Li et al. (2016), Ruiz et al. (2016), Okuwaki et al. (2016) and Shrivastava et al. (2016), and the best

fit was selected according to tide gauges in Coquimbo, Valparaiso and the nearest DART buoy. The model proposed by Li et al. (2016) is obtained from iterative modeling of teleseismic body waves as well as tsunami records at DART buoys. Since the magnitude of the proposed model is Mw 8.21, the slip distribution was multiplied by a factor of 1.38; thus, all events have the same magnitude: 8.3.

5   The tsunami initial condition was estimated to be equal to the seafloor displacement. In addition, the vertical displacement from each subfault was computed using a kinematic solution of the planar fault model of Okada (Okada, 1985). The numerical simulations were carried out with the Non-hydrostatic Evolution of Ocean WAVEs model (NEOWAVE) (Yamazaki et al. 2011; Yamazaki et al., 2009). This model is a staggered finite difference model which solves the nonlinear shallow water equation and considers a vertical velocity term to account for weakly dispersive waves. The model generates the tsunami initial

10   condition, propagation and inundation by means of several nested grids of different resolutions. The present research used 5 nested grids, as shown in Figure 4. The level 1 grid describes tsunami propagation from generation to the continental shelf and to the Pacific Ocean at a resolution of 2 arcmin (~3600m). This grid was generated from 30 arcmin GEBCO data. The level 2 and level 3 grids were built from nautical charts data and had a resolution of 30 and 6 arcsec, respectively. The level 4 grid covered Coquimbo Bay and was also built from nautical charts with a resolution of 1 arcsec (~30m). Finally, the level 5 grid

15   had a resolution of 1/3 arcsec (~10m) and was built from bathymetry of nautical charts and topography from a detailed DTM provided by the Ministry of Public Works (MINVU) in Coquimbo. The topography used high-resolution data; thus, the most important features such as the coastal road embankment, railway, river and wetland are well represented (see Figure 4, grid 5). Numerical simulations in Valparaiso considered four nested grids with a maximum grid resolution of 1 arcsec (~30 m).

The roughness coefficient was defined as n=0.025 at the seabed, as recommended for tsunamis (Bricker et al., 2015; Kotani et

20   al., 1998). However, in coastal, wetland and urban areas, we tested several roughness coefficient values (Bricker et al., 2015) in order to obtain the best fit of tsunami inundation height. The validation of the numerical simulation was performed using the Root Mean Square Error and the parameters K and κ given by equations (1) and (2)(Gokon et al., 2014; Suppasri et al., 2011) . The variable K_i is defined as $K_i = x_i/y_i$, where x_i and y_i are recorded and computed tsunami heights, respectively. The Japan Society of Civil Engineering provides guidelines, which recommend that $0.95 < K < 1.05$ and $\kappa < 1.45$ to be

25   considered "good agreement" (Gokon et al., 2014).

$$\log K = \frac{1}{n}\sum_{i=1}^{n} \log K_i, \tag{1}$$

$$\log \kappa = \sqrt{\frac{1}{n}\sum_{i=1}^{n} (\log K_i)^2 - (\log K)^2}, \tag{2}$$

Figure 5 shows the tsunami initial conditions of the four slip models and the tsunami waveforms of an elapsed time of 4 hours at three selected gauges, namely, Coquimbo, Valparaiso and DART buoy 32402. Even though the modified Li et al., (2016)

30   model overestimates the maximum amplitude at the DART buoy, the simulation shows a very good agreement with the tsunami record in Coquimbo. When the Mw 8.3 models proposed by Ruiz et al. (2016) and Shrivastava et al. (2016) were analyzed, it was possible to observe a good agreement at the DART buoy and Valparaiso tide gauge; however, the amplitude in Coquimbo is underestimated by more than a meter. The Okuwaki et al. (2016) model overestimates both the DART buoy and Valparaiso

tide gauge, despite the second tsunami wave reaching a similar amplitude in Coquimbo. Nevertheless, the maximum tsunami amplitude is underestimated. Therefore, the modified Li et al. (2016) model is selected to assess the suitable Manning roughness coefficient.

Figure 6 shows the inundation area and tsunami inundation height results obtained from the numerical simulations of the Li et al. (2016) model with four different roughness coefficients. The tested coefficients are n=0.025 for coastal and riverine areas, 0.04 and 0.05 for low-density urban areas and 0.06 for medium-density urban areas (Bricker et al., 2015). From the figure, it is possible to observe that the best fit is obtained for n=0.025, which resulted in $K = 1.05$ and $\kappa < 1.45$, corresponding to "good agreement." For higher roughness coefficients, the tsunami inundation heights are underestimated. In addition, the larger the coefficient, the smaller the inundation area. This behavior could be explained by the fact that a significant part of the flooded area is a wetland and the developed area is rather small, with a low-density residential distribution. Subsequently, the inundation depth is computed from the inundation area given by the modified Li et al. (2016) slip model with a roughness coefficient of n=0.025.

3.3 Fragility curve

The construction of a fragility curve requires a correlation between the structural damage level to the hydrodynamic features of a tsunami such as the flow depth, current velocity and hydrodynamic force (Koshimura et al., 2009). Since the velocity is difficult to be measured during tsunami and validated by numerical models, we used the tsunami inundation depth to develop the fragility curve. To this end, a sample size is defined such that each range of the interpolated inundation depth includes the defined number of structures. Then, the damage probability is calculated by counting the number of destroyed or surviving structures for each range of inundation depth. Finally, the fragility function is developed by the regression analysis of the discrete set of the damage probabilities and inundation depths. Therefore, it is assumed that the cumulative probability P of occurrence of damage follows the standardized normal or lognormal distribution function given in equation (3). Φ is the distribution function, x is the inundation depth of the tsunami and μ and σ are the mean and standard deviation of x, respectively. The values of μ and σ are calculated by means of least-squares fitting of x and the inverse of Φ, (Φ^{-1}) on normal paper given by equation (4).

$$P(x) = \Phi\left[\frac{x-\mu}{\sigma}\right], \tag{3}$$

$$x = \sigma\Phi^{-1} + \mu, \tag{4}$$

Figure 7 shows the tsunami inundation depth and the results of the tsunami fragility curve of Coquimbo. The sample size was defined to be 40 structures; thus, 15 inundation depth ranges were used. Figure 7b shows the histogram, while Figure 7d shows the relationship between damage probability and inundation depth, with the solid line being the best-fit curve of the plot. The fragility curve was estimated by means of regression analysis, as shown in Figure 7c. The values of μ and σ were found to be 2.4395 and 0.5537, respectively, with a correlation factor $R^2 = 0.852$. It is possible to observe that flow depths lower than 1.5 m did not generate damage to the surveyed structures and the damage probability of the curve is lower than 10%. Moreover,

the fragility curve shows that flow depths higher than 4 m could cause 100% of severe damage to mixed structures in Coquimbo. Thus, it becomes very important to assess the tsunami damage due to possible events taking place in the same rupture area as that of the 1922 earthquake, since large inundation depths were reported there (see section 2).

3.3 Fragility curve

This section compares the fragility curve obtained in Coquimbo with other curves obtained in other places after recent events. Statistical parameters of existing fragility curves are shown in Table 1. One curve is that of Okushiri, Japan, which was obtained for wooden structures after the 1993 tsunami event. The analysis included 523 houses and a range of approximately 50 structures (Suppasri et al., 2012). In a similar manner, the fragility curve of Dichato, Chile, considered 915 structures of mixed materials and a range of 50 structures after the 2010 Chile tsunami (Mas et al., 2012). A more comprehensive analysis was conducted in Banda Aceh, Indonesia, after the Indian Ocean Tsunami (Koshimura et al., 2009). This case considered 48,910 structures of wood, timber and reinforced concrete with a range of 1,000 structures. The comparison with the Coquimbo fragility curve is shown in Figure 8a. It is seen that Coquimbo experienced less damage than Dichato and Okushiri for inundation depths lower than 3 m. In fact, for an inundation depth of 2 m, Dichato and Okushiri have a 68-75% probability of damage, while in Coquimbo it is only 20%. The high probability of damage in Dichato and Okushiri is due to the large number of structures made of wood and lightweight materials that have little resistance to tsunami flows (Mas et al., 2012). Even though the building materials in Coquimbo are similar, it is believed that the distant from shore and railway embankment can decrease tsunami energy (see Figure 3); thus, the same inundation depth generates less damage to structures. In a similar manner, Banda Aceh has a low probability of damage (<20%) for an inundation depth of 2 m. However, the damage probability in Coquimbo increases rapidly as the inundation depth increases, reaching a 100% probability of damage for an inundation depth of only 4 m, which could be because most of the houses have only 1 or 2 stories (see Figure 2). Figures 8b and c show the comparison of the Coquimbo fragility curve with the curves given by Suppasri et al. (2013) for wooden and mixed materials in Japan, respectively. The study considered more than 250,000 damaged buildings surveyed after the 2011 Great East Japan Tsunami and made it possible to analyze different damage levels and building materials. In general, it is seen that wooden and mixed structures in Japan have similar behavior. If damage level 4 (complete damage) is analyzed, the damage probability is higher than in Coquimbo for an inundation depth lower than 2 m. Similar to the case of Dichato and Okushiri, wooden and mixed structures in Japan have a relatively high probability of complete damage (level 4), ranging from 50 to 60%, while in Coquimbo it is only 20%. Another group of fragility curves is shown in Figures 8d and e for wooden and mixed structures, respectively, which were obtained from survey data of the 2011 Japan tsunami in the Sendai and Ishinomaki plains (Suppasri et al., 2012). Theses curves show that structures located in flat areas are less impacted by tsunami despite large inundation depths, in contrast to what happened in areas with ria topography such as the Sanriku coast (Suppasri et al., 2013; Suppasri et al., 2012) and semi-closed bays such as Dichato (Mas et al., 2012). This behavior is in good agreement with damage observed in the Coquimbo area, where the flat area and distant from shore could decrease tsunami impact. However, from Figure 8d, it

is possible to observe that the Coquimbo fragility curve (destroyed or complete damage) overlaps with the minor damage level curve for wood and mixed material houses in flat areas in Japan. A possible explanation is that houses in Japan are relatively new and built according to strict construction standards (Suppasri et al., 2012), in contrast to what was observed in Coquimbo where old houses are found (See Figure 2). This finding suggests that topography as well as structure quality should be

5   considered in tsunami damage estimation.

4 Application of fragility curve to tsunami damage estimation

This section presents an example of the use of fragility curves to estimate tsunami damage by a deterministic tsunami scenario in Coquimbo. We first define a tsunami scenario, then we run the numerical simulation to obtain the inundation depth and, finally, we estimate the tsunami damage in Coquimbo. Since damage due to earthquake in Coquimbo Region was limited in

10   2015 (Candia et al., 2017; Fernández et al., 2017), it is assumed that the damage to structures is exclusively due to tsunami.

4.1. Tsunami source model

Based on Figure 1, three possible segments can be defined, namely, the Copiapó-Coquimbo, Coquimbo-Illapel and Illapel-Constitución regions. However, events in the Illapel-Constitución region, including those of 1822 and 1906, have never

15   generated a tsunami in Coquimbo (Soloviev & Go, 1975). Only the 1730 event, which ruptured the Coquimbo-Illapel segment, generated a tsunami in the area of interest (Cisternas et al., 2011). Therefore, possible tsunamis generated in the Valparaiso segment were not considered in the present analysis. In a similar manner, earthquakes on the Coquimbo-Illapel segment were not considered as the 2015 event filled the seismic gap that had existed since the last major earthquake in 1943 or earlier events (Ye et al., 2016); therefore, no significant earthquakes that generate significant tsunamis could take place there in the near

20   future. Conversely, the northern segment has shown no relevant seismic activity since 1922, i.e., 95 years before 2017 (see Figure 1). Moreover, the previous significant event took place in 1819 (73 years before the 1922 event). Therefore, the Copiapó-Coquimbo segment is of particular interest regarding possible future earthquakes and tsunamis in Coquimbo.

It is important to note that the small event in 1849 (magnitude 7.5, according to Lomnitz (2004)) generated a 5-m tsunami in Coquimbo. In addition, the 1922 Atacama event had a complex source of three shocks clustered in time (Beck et al., 1998).

25   Therefore, it seemed reasonable to separate the northern segments into two different seismic regions, with one segment covering Copiapó to Punta Choros (Figure 9b) and the second segment from Punta Choros to Ovalle (Figure 9a), which coincides with the estimated rupture length of the 1849 event (see Figure 1).

The tsunami hazard assessment and damage estimation could use either a probabilistic or deterministic approach. While the former takes into account many uncertainties related to generation, propagation and inundation (Cheung et al., 2011; Geist &

30   Parsons, 2006; Heidarzadeh & Kijko, 2011; Horspool et al., 2014; Park & Cox, 2016), the latter uses credible worst-case scenarios based on historical events (Aránguiz et al., 2014; Mitsoudis et al., 2012; Wijetunge, 2012). However, the coupling

coefficient could be used to assess the shape of possible future deterministic earthquakes (Métois et al., 2016; Pulido et al., 2015) since reasonable heterogeneous slip models could be predicted by the interseismic degree of locking (Calisto et al., 2016; Gonzalez-Carrasco et al., 2015). Thus, the slip distribution S at arbitrary space ξ is represented as given by equation (5):

$$S(\xi) = \int_{t_0}^{t_1} C(\xi, t)V(\xi)dt - \sum_j \big(s_j(\xi) + p_j(\xi)\big), \tag{5}$$

5 where C is the interseismic coupling, ranging from 0 to 1. The interseismic coupling model adopted in this study is from Métois et al., (2016), which is derived from inverting Global Positioning System (GPS) measurements along the Chilean margin (18–38°S) that have been conducted by international teams since the early 1990s (see Métois et al., (2016) and references therein). It provides a reasonable estimate of the degree of locking between the Nazca and the South American plates, indicating strong coupling along the scenario source regions (See Figures 9d to f). V is the plate convergence rate at ξ

10 derived from the NNR-Nuvel1A model (DeMets et al., 1994) and t_0 and t_1 delimit the interseismic period for integration. s_j is the slip of the small event ($4.8 \leq \mathrm{Mw} \leq 7.9$) at the jth location, which is listed in the Global Centroid Moment Tensor (GCMT) Catalog (http://www.globalcmt.org/CMTsearch.html, see Figure 9e), and p_j is the post-seismic slip following s_j. Each amount of slip s_j is calculated based on the seismic moment obtained by the GCMT and the empirical relationship between rupture area and the moment magnitude introduced by Wells & Coppersmith (1994). The rigidity modulus for the

15 calculation of moment magnitude of each s_j is computed with the layered, near-source structure adopted in the source study by Okuwaki et al. (2016). We eliminated the Mw 8.3 2015 Illapel earthquake from the GCMT list and instead considered its contribution to the scenario source models with the inverted slip model by Okuwaki et al. (2016) in equation (5) (Fig. 9). The slip motion of S is assumed to be pure thrust against the subducting plate motion. Note that C is constant against time and the post-seismic slip p_j is not considered in the present analysis; thus, it is possible that the scenario source models will slightly

20 overestimate S.

The variable slip distribution was obtained from the heterogeneous interseismic coupling C. Time intervals for the integral of equation (5) are assumed to be 94 years (1922 to 2016). Each segment is subdivided into 10 km x 10 km sub-space knots for 150 x 160 km2 and 180 x 160 km2 source areas for S1 and S2, respectively. The strike and dip angles for the scenario source geometry are assumed to be constant based on the subducting slab geometry of the Slab 1.0 model (Hayes et al., 2012): (Strike,

25 Dip) = (2.7°, 15.0°) for S1 and (Strike, Dip) = (16.0°, 15.0°) for S2. The fault geometry and characteristic source parameters as well as complete model parameters for each scenario source model are available from the authors upon request.

4.2 Numerical simulation of proposed tsunami scenario

The computation covered an elapsed time of 6 hours with output intervals of 1 min. Figure 10 shows the main results and the

30 three different combinations of tsunami scenarios. The upper row shows the results for segment S1 (Mw 8.2) and the central row shows the results for segment S2 (Mw 8.4), while the lower row shows the results for the combined scenario of S1 and S2 (Mw 8.5). In addition, the left column shows the vertical displacement of the seafloor, the central column shows the

maximum flow depth and the right column shows the tsunami wave form at the Coquimbo tide gauge during an elapsed time of 4 hours (240 min). It is observed that segment S2 (Mw 8.4) generated lower inundation depths than segment S1 (Mw 8.2), which can be explained by the fact that the strike angle and the coastal morphology make the tsunami propagate toward the north and not directly toward Coquimbo Bay. Meanwhile, the tsunami generated by segment S1, the second wave of which is

5   the largest, propagates directly toward Coquimbo Bay. It is possible to observe that the maximum inundation depths reached up to 5m in developed areas and along the coastline. Moreover, it is interesting that the Mw 8.5 event, as a combination of S1 and S2 (lower row in Figure 10), generated lower inundation depths than segment S1 alone. This can be explained by the fact that the maximum tsunami amplitude of each individual event does not take place at the same time; subsequently, the tsunami from segment S2 decreases the maximum amplitude of the tsunami from segment S1. Larger tsunami amplitudes could be

10   obtained if there is a time difference between segments S1 and S2 such that the maximum tsunami waves coincide. Nevertheless, this analysis is beyond the scope of the present paper.

4.3 Damage to structures

The previous section demonstrated that the combination of S1 and S2 rupturing at the same time generated lower inundation

15   heights than S1 alone. Therefore, the damage to structures is assessed for segment S1 only, i.e., a tsunami generated by a Mw 8.2 earthquake off the coast of Coquimbo, which generates inundation heights lower than 5 m. In order to determine a high or low probability of damage to a given structure, first the latitude and longitude coordinates are assigned to each structure within the inundation area, and the maximum flow depths given by the tsunami numerical simulation at the location of each structure are exported to GIS. Second, the flow depth database is divided into several ranges, with 40 samples in each range, and the

20   mean value of each range is intersected with the fragility curve given in Figure 7c in order to define the damage probability for each range. Third, the damage probability given in the previous step is assumed to be equal to the percentage of structures with a high probability of damage within each range. To do this, the inundation depths for each range are arranged in descending order and the structures outside of that percentage (with the lowest flow depth within the range) are assumed to have a low probability of damage.

25   Figure 11a shows the low area of the city of Coquimbo and the computed flow depth given by the numerical simulation of scenario S1. 646 structures of mixed construction materials were identified within the inundation area, and they are colored according to flow depth level. Figure 11b shows the result of the damage estimation. It was found that 321 structures, i.e., 49.6% of the flooded structures, have a high probability of damage, a figure that is much larger than the 20% surveyed right after the 2015 tsunami. As expected, the structures behind the railway embankment and wetland would experience less damage

30   than structures located close to the shore. Due to the high probability of damage to houses located close to the shore, it is recommended that any reconstruction plan or future tsunami mitigation measures consider the fact that high tsunami inundation depths (5-8 m) could be generated in this area.

5 Conclusions

Numerical simulations of the 2015 Chile tsunami proved to be in good agreement with field survey data in Coquimbo. A fragility curve of Coquimbo was developed with two-level classification of structural damage, namely, "surviving" and "destroyed." The Coquimbo fragility curve shows a low probability of damage, 20%, at a relatively high inundation depth (2m), in contrast to what was observed in another Chilean town, Dichato, where a 68% probability of damage is obtained for the same inundation depth. This result is in good agreement with fragility curves in the Sendai and Ishinomaki plains in Japan, such that tsunami energy was decreased and less damage was observed. Future research may include other hydrodynamic features such as velocity or hydrodynamic force, even the development of fragility surface.

The fragility curve may be used to estimate possible future tsunami damage in the Coquimbo and other places with similar topography and structure material. In Coquimbo, it was found that a Magnitude Mw 8.2 earthquake off the coast of Coquimbo could generate a destructive tsunami with flow depths of up to 5 m. The assessment of tsunami damage with the fragility curve demonstrated that ~50% of the structures have a high probability of damage if the reconstruction is carried out with the same types of structures, which is greater than the damage caused by the 2015 tsunami (20%). Therefore, the tsunami mitigation measures and the reconstruction plan should consider the potential tsunami damage due to a future earthquake off the coast of Coquimbo. It is recommended that new land use policies be implemented in order to regulate the type of structures being built in the inundation area.

References

Aránguiz, R., González, G., González, J., Catalán, P., A., Cienfuegos, R., Yagi, Y., … Rojas, C. (2016). The 16 September 2015 Chile Tsunami from the Post-Tsunami Survey and Numerical Modeling Perspectives. *Pure and Applied Geophysics*, *173*(2), 333–348. http://doi.org/10.1007/s00024-015-1225-4

Aránguiz, R., Shibayama, T., & Yamazaki, Y. (2014). Tsunamis from the Arica-Tocopilla source region and their effects on ports of Central Chile. *Natural Hazards*, *71*(1), 175–202. JOUR. http://doi.org/10.1007/s11069-013-0906-5

Beck, S., Barrientos, S., Kausel, E., & Reyes, M. (1998). Source characteristics of historic earthquakes along the central Chile subduction zone. *Journal of South American Earth Science*, *11*(2), 115–129.

Bricker, J. D., Gibson, S., Takagi, H., & Imamura, F. (2015). On the Need for Larger Manning' s Roughness Coefficients in Depth-Integrated Tsunami Inundation Models. *Coastal Engineering Journal*. http://doi.org/10.1142/S0578563415500059

Calisto, I., Miller, M., & Constanzo, I. (2016). Comparison Between Tsunami Signals Generated by Different Source Models and the Observed Data of the Illapel 2015 Earthquake. *Pure and Applied Geophysics*, *173*(4), 1051–1061. http://doi.org/10.1007/s00024-016-1253-8

Candia, G., de Pascale, G. P., Montalva, G., & Ledezma, C. (2017). Geotechnical Aspects of the 2015 Mw 8.3 Illapel Megathrust Earthquake Sequence in Chile. *Earthquake Spectra*, *33*(2), 709–728. JOUR. http://doi.org/10.1193/031716EQS043M

Cheung, K. F., Wei, Y., Yamazaki, Y., & Yim, S. C. S. (2011). Modeling of 500-year tsunamis for probabilistic design of coastal infrastructure in the Pacific Northwest. *Coastal Engineering*, *58*(10), 970–985. http://doi.org/10.1016/j.coastaleng.2011.05.003

Cisternas, M., Gorigoitía, N., Torrejón, F., & Urbina, X. (2011). Terremoto y tsunami de Chile central de 1730: .Un gigante o una serie de eventos menores? In *XXXI Congreso de Ciencias del Mar*.

Contreras-López, M., Winckler, P., Sepúlveda, I., Andaur-Álvarez, A., Cortés-Molina, F., Guerrero, C. J., … Figueroa-Sterquel, R. (2016). Field Survey of the 2015 Chile Tsunami with Emphasis on Coastal Wetland and Conservation Areas. *Pure and Applied Geophysics*, *173*(2), 349–367. http://doi.org/10.1007/s00024-015-1235-2

DeMets, C., Gordon, R. G., Argus, D. F., & Stein, S. (1994). Effect of recent revisions to the geomagnetic reversal time scale on estimates of current plate motions. *Geophysical Research Letters*, *21*(20), 2191–2194. JOUR. http://doi.org/10.1029/94GL02118

Dengler, L., Borrero, J., Gelfenbaum, G., Jaffe, B., Okal, E., Ortiz, M., … Ocala, L. (2003). Tsunami. *Earthquake Spectra*, *19*(S1), 115–144. JOUR. http://doi.org/10.1193/1.1737247

Dominey-Howes, D., Dengler, L., Dunbar, P., Kong, L., Fritz, H., Imamura, F., … Yamamoto, M. (2012). *International tsunami survey team (ITST) post-tsunami survey field guide* (JOUR). *UNESCO-IOC, Paris*.

Fernández, J., Pastén, C., Ruiz, S., & Leyton, F. (2017). Estudio de efectos de sitio en la Región de Coquimbo durante el terremoto de Illapel Mw 8.3 de 2015. *Obras Y Proyectos*, (21), 20–28.

Fuentes, M. A., Riquelme, S., Hayes, G. P., Medina, M., Melgar, D., Vargas, G., … Villalobos, A. (2016). A Study of the 2015 M w 8.3 Illapel Earthquake and Tsunami: Numerical and Analytical Approaches. *Pure and Applied Geophysics*. http://doi.org/10.1007/s00024-016-1305-0

Geist, E. L., & Parsons, T. (2006). Probabilistic analysis of tsunami hazards. *Natural Hazards*, *37*(3), 277–314.

Gokon, H., Koshimura, S., Imai, K., Matsuoka, M., Namegaya, Y., & Nishimura, Y. (2014). Developing fragility functions for the areas affected by the 2009 Samoa earthquake and tsunami. *Nat. Hazards Earth Syst. Sci., 14*, 3231–3241. http://doi.org/10.5194/nhess-14-3231-2014

Gonzalez-Carrasco, J., Aránguiz, R., Dominguez, J., C., & Urra, L. (2015). Assessment of interseismic coupling models to

estímate inundation and runup. In *Seismological Research Letters* (pp. 665–666).

Hayes, G. P., Wald, D. J., & Johnson, R. L. (2012). Slab1.0: A three-dimensional model of global subduction zone geometries. *Journal of Geophysical Research: Solid Earth*, *117*(B1), n/a-n/a. JOUR. http://doi.org/10.1029/2011JB008524

Heidarzadeh, M., & Kijko, A. (2011). A probabilistic tsunami hazard assessment for the Makran subduction zone at the northwestern Indian Ocean. *Natural Hazards*, *56*(3), 577–593. JOUR. http://doi.org/10.1007/s11069-010-9574-x

Horspool, N., Pranantyo, I., Griffin, J., Latief, H., Natawidjaja, D. H., Kongko, W., … Thio, H. K. (2014). A probabilistic tsunami hazard assessment for Indonesia. *Nat. Hazards Earth Syst. Sci.*, *14*(11), 3105–3122. JOUR. http://doi.org/10.5194/nhess-14-3105-2014

Koshimura, S., Namegaya, Y., & Yanagisawa, H. (2009). Tsunami fragility: A new measure to identify tsunami damage. *Journal of Disaster Research*, *4*(6), 479–488. Retrieved from http://www.fujipress.jp/finder/xslt.php?mode=present&inputfile=DSSTR000400060013.xml

Koshimura, S., Oie, T., Yanagisawa, H., & Imamura, F. (2009). Developing Fragility Functions for Tsunami Damage Estimation Using Numerical Model and Post-Tsunami Data From Banda Aceh, Indonesia. *Coastal Engineering Journal*, *51*(3), 243–273. http://doi.org/10.1142/S0578563409002004

Koshimura, S., Oie, T., Yanagisawa, H., Imamura, F., Oie, T., Yanagisawa, H., & Imamura, F. (2009). Developing Fragility Functions for Tsunami Damage Estimation Using Numerical Model and Post-Tsunami Data From Banda Aceh, Indonesia. *Coastal Engineering Journal*, *51*(3), 243–273. http://doi.org/10.1142/S0578563409002004

Kotani, M., Imamura, F., & Shuto, N. (1998). Tsunami runup simulation and damage estimation by using geographical information system. In *Proceedings of Coastal Engineering JSCE* (p. vol 45 pp356-360).

Li, L., Lay, T., Cheung, K. F., & Ye, L. (2016). Joint modeling of teleseismic and tsunami wave observations to constrain the 16 September 2015 Illapel, Chile M w 8.3 earthquake rupture process. *Geophysical Research Letters*, (September 2015), 4303–4312. http://doi.org/10.1002/2016GL068674

Lomnitz, C. (2004). Major Earthquakes of Chile: A Historical Survey, 1535-1960. *Seismological Research Letters*, *75*(3), 368–378. http://doi.org/10.1785/gssrl.75.3.368

Mas, E., Koshimura, S., Suppasri, A., Matsuoka, M., Matsuyama, M., Yoshii, T., … Imamura, F. (2012). Developing Tsunami fragility curves using remote sensing and survey data of the 2010 Chilean Tsunami in Dichato. *Natural Hazards and Earth System Science*, *12*(8), 2689–2697. http://doi.org/10.5194/nhess-12-2689-2012

Melgar, D., Fan, W., Riquelme, S., Geng, J., Liang, C., Fuentes, M., … Fielding, E. J. (2016). Slip segmentation and slow rupture to the trench during the 2015, Mw8.3 Illapel, Chile earthquake. *Geophysical Research Letters*. http://doi.org/10.1002/2015GL067369

Métois, M., Vigny, C., & Socquet, A. (2016). Interseismic Coupling, Megathrust Earthquakes and Seismic Swarms Along the Chilean Subduction Zone (38{\textdegree}--18{\textdegree}S). *Pure and Applied Geophysics*, *173*(5), 1431–1449. http://doi.org/10.1007/s00024-016-1280-5

Mitsoudis, D. A., Flouri, E. T., Chrysoulakis, N., Kamarianakis, Y., Okal, E. A., & Synolakis, C. E. (2012). Tsunami hazard

in the southeast Aegean Sea. *Coastal Engineering*, *60*(1), 136–148. http://doi.org/10.1016/j.coastaleng.2011.09.004

Nandasena, N. A. K., Sasaki, Y., & Tanaka, N. (2012). Modeling field observations of the 2011 Great East Japan tsunami: Efficacy of artificial and natural structures on tsunami mitigation. *Coastal Engineering*, *67*, 1–13. http://doi.org/10.1016/j.coastaleng.2012.03.009

Nishenko, S. P. (1985). Seismic potential for large and great interplate earthquakes along the Chilean and Southern Peruvian Margins of South America: A quantitative reappraisal. *Journal of Geophysical Research*, *90*(B5), 3589–3615. http://doi.org/10.1029/JB090iB05p03589

Nistor, I., Palermo, D., Nouri, Y., Murty, T., & Saatcioglu, M. (2009). Tsunami-Induced Forces on Structures. In C. Y. Kim (Ed.), *Handbook of Coastal and Ocean Engineering* (pp. 261–286). World Scientific. http://doi.org/10.1142/9789812819307_0011

Okada, Y. (1985). Surface deformation due to shear and tensile faults in a half space. *Bulletin of the Seismological Society of America*, *75*(4), 1135–1154.

Okuwaki, R., Yagi, Y., Aránguiz, R., González, J., & González, G. (2016). Rupture Process During the 2015 Illapel, Chile Earthquake: Zigzag-Along-Dip Rupture Episodes. *Pure and Applied Geophysics*, *173*(4), 1011–1020. http://doi.org/10.1007/s00024-016-1271-6

Park, H., & Cox, D. T. (2016). Probabilistic assessment of near-field tsunami hazards: Inundation depth, velocity, momentum flux, arrival time, and duration applied to Seaside, Oregon. *Coastal Engineering*, *117*, 79–96. http://doi.org/10.1016/j.coastaleng.2016.07.011

Park, H., Cox, D. T., & Barbosa, A. R. (2017). Comparison of inundation depth and momentum flux based fragilities for probabilistic tsunami damage assessment and uncertainty analysis. *Coastal Engineering*, *122*, 10–26. http://doi.org/10.1016/j.coastaleng.2017.01.008

Pulido, N., Aguilar, Z., Tavera, H., Chlieh, M., Calderón, D., Sekiguchi, T., … Yamazaki, F. (2015). Scenario Source Models and Strong Ground Motion for Future Mega- earthquakes: Application to Lima, Central Peru. *Bulletin of the Seismological Society of America* . JOUR. Retrieved from http://www.bssaonline.org/content/early/2015/01/06/0120140098.abstract

Ruiz, S., Klein, E., DelCampo, F., Rivera, E., Poli, P., Metois, M., … Fleitout, L. (2016). The Seismic Sequence of the 16 September 2015 Mw 8.3 Illpel, Chile, Earthquake. *Seismological Research Letters*, *87*(July/August 2016), 789–799. http://doi.org/10.1785/0220150281

Shimozono, T., & Sato, S. (2016). Coastal vulnerability analysis during tsunami-induced levee overflow and breaching by a high-resolution flood model. *Coastal Engineering*, *107*, 116–126. http://doi.org/10.1016/j.coastaleng.2015.10.007

Shrivastava, M. N., González, G., Moreno, M., Chlieh, M., Salazar, P., Reddy, C. D., … delaLlera, J. C. (2016). Coseismic slip and afterslip of the 2015 Mw 8.3 Illapel (Chile) earthquake determined from continuous GPS data. *Geophysical Research Letters*, *43*. http://doi.org/10.1002/2016GL070684

Soloviev, S. ., & Go, C. N. (1975). *A Catalogue of Tsunamis on the Eastern Shore of the Pacific Ocean*. Moscow: Nauka

Publishing House.

Suppasri, A., Koshimura, S., & Imamura, F. (2011). Developing tsunami fragility curves based on the satellite remote sensing and the numerical modeling of the 2004 Indian Ocean tsunami in Thailand. *Natural Hazards and Earth System Science*, *11*(1), 173–189. http://doi.org/10.5194/nhess-11-173-2011

5 Suppasri, A., Koshimura, S., Matsuoka, M., Gokon, H., & Kamthonkiat, D. (2012). Application of Remote Sensing for Tsunami Disaster. In *Remote Sensing of Planet Earth*. InTech.

Suppasri, A., Mas, E., Charvet, I., Gunasekera, R., Imai, K., Fukutani, Y., … Imamura, F. (2013). Building damage characteristics based on surveyed data and fragility curves of the 2011 Great East Japan tsunami. *Natural Hazards*, *66*(2), 319–341. http://doi.org/10.1007/s11069-012-0487-8

10 Suppasri, A., Mas, E., Koshimura, S., Imai, K., Harada, K., & Imamura, F. (2012). Developing Tsunami Fragility Curves From the Surveyed Data of the 2011 Great East Japan Tsunami in Sendai and Ishinomaki Plains. *Coastal Engineering Journal*, *54*(116), 1–16. http://doi.org/10.1142/S0578563412500088

Synolakis, C. E., & Okal, E. A. (2005). 1992–2002: Perspective on a Decade of Post-Tsunami Surveys BT - Tsunamis: Case Studies and Recent Developments. In K. Satake (Ed.) (pp. 1–29). CHAP, Dordrecht: Springer Netherlands.
15 http://doi.org/10.1007/1-4020-3331-1_1

Wei, Z., Dalrymple, R. A., H??rault, A., Bilotta, G., Rustico, E., & Yeh, H. (2015). SPH modeling of dynamic impact of tsunami bore on bridge piers. *Coastal Engineering*, *104*, 26–42. http://doi.org/10.1016/j.coastaleng.2015.06.008

Wells, D. L., & Coppersmith, K. J. (1994). New empirical relationships among magnitude, rupture length, rupture width, rupture area, and surface displacement. *Bulletin of the Seismological Society of America* , *84*(4), 974–1002. JOUR.
20 Retrieved from http://www.bssaonline.org/content/84/4/974.abstract

Wijetunge, J. J. (2012). Nearshore tsunami amplitudes off Sri Lanka due to probable worst-case seismic scenarios in the Indian Ocean. *Coastal Engineering*, *64*, 47–56. http://doi.org/10.1016/j.coastaleng.2012.02.005

Yamazaki, Y., Cheung, K. F., & Kowalik, Z. (2011). Depth-integrated, non-hydrostatic model with grid nesting for tsunami generation, propagation, and run-up. *International Journal for Numerical Methods in Fluids*, *67*(12), 2081–2107. JOUR.
25 http://doi.org/10.1002/fld.2485

Yamazaki, Y., Kowalik, Z., & Cheung, K. F. (2009). Depth-integrated, non-hydrostatic model for wave breaking and run-up. *International Journal for Numerical Methods in Fluids*, *61*(5), 473–497. JOUR. http://doi.org/10.1002/fld.1952

Ye, L., Lay, T., Kanamori, H., & Koper, K. D. (2016). Rapidly Estimated Seismic Source Parameters for the 16 September 2015 Illapel, Chile Mw 8.3 Earthquake. *Pure and Applied Geophysics*, *173*(2), 321–332. http://doi.org/10.1007/s00024-
30 015-1202-y

Natural Hazards
and Earth System
Sciences
Discussions

Table 1. Summary of statistical parameters and damage levels for empirical fragility curves (Mas et al., 2012; Suppasri et al., 2013; Suppasri et al., 2012) including the current Coquimbo case. μ and σ are statistical parameters for normal distribution, while μ' and σ' are the same parameters for lognormal distribution

Event	Location	Structure type	Damage level	No. structures inspected	μ	σ	μ'	σ'	R^2
Chile (2015)	Coquimbo-Chile	Wood, masonry, mixed	Surviving/ destroyed	568	2.4395	0.5537			0.852
Chile (2010)	Dichato-Chile	Wood, masonry, mixed	Surviving/ destroyed	915			0.092	1.272	0.86
Japan (2011)	Okushiri-Japan	Wood	Surviving/ destroyed	523			0.216	0.736	0.82
Indian Ocean (2004)	Banda Aceh-Indonecia	Wood, timber, RC	Surviving/ destroyed	48,910	2.985	1.117			0.99
Japan (2011)	Hokkaido, Aomori, Iwate, Miyagi, Fukushima, Ibaraki, Chiba	Wood	Level 1	251,000 (total)			-2.1216	1.2261	0.98
			Level 2				-0.9338	0.9144	0.98
			Level 3				-0.040	0.7276	0.98
			Level 4				0.6721	0.4985	0.98
			Level 5				0.7825	0.5559	0.98
			Level 6				1.2094	0.5247	0.97
Japan (2011)	Hokkaido, Aomori, Iwate, Miyagi, Fukushima, Ibaraki, Chiba	Mix	Level 1	251,000 (total)			-2.4562	1.4874	0.99
			Level 2				-1.1373	1.115	0.96
			Level 3				-0.0756	0.8277	0.97
			Level 4				0.5316	0.6235	0.91
			Level 5				0.8336	0.6077	0.97
			Level 6				1.2244	0.5723	0.98
Japan (2011)	Ishinomaki and Sendai plains	Wood	minor	150	2.4409	0.6409			0.95
			moderate		2.9028	0.6777			0.94
			major		3.8458	0.8516			0.95
			complete		4.2243	1.0159			0.80
Japan (2011)	Ishinomaki and Sendai plains	Mix	minor	189	2.4954	0.8249			0.81
			moderate		3.2550	1.0647			0.80
			major		4.4355	1.3068			0.83
			complete		5.0620	1.4872			0.84
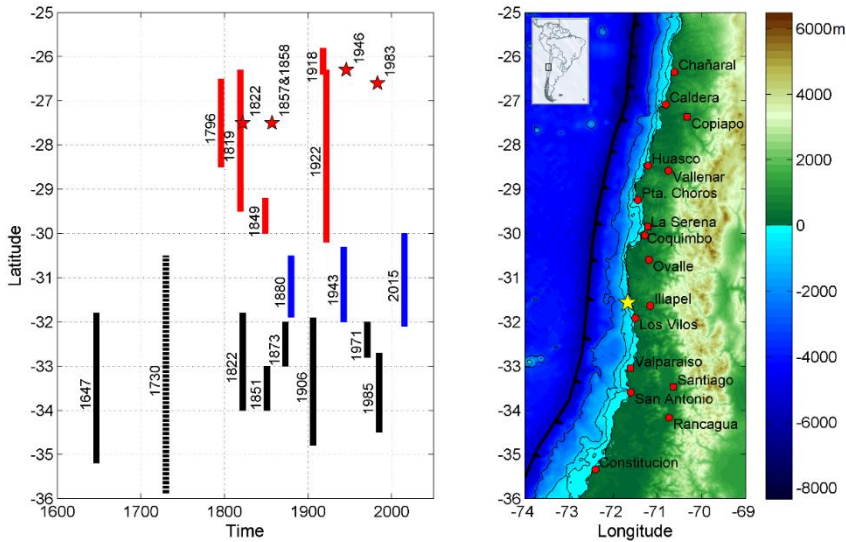
5

Figure 1: Seismicity of central Chile. Left: Space-time plot of large earthquakes along central Chile. Red bars are the events along the Copiapó-Coquimbo region and the red stars represent smaller seismic events. The blue bars are events along the Coquimbo-Illapel seismic region, while the black lines represent events along the Los Vilos-Constitución segment. The dashed line is the large
5 **event of 1730, which ruptured both the Los Vilos-Constitución and Coquimbo-Illapel segments. (Beck et al., 1998; Lomnitz, 2004; Métois et al., 2016; Nishenko, 1985). Right: Map showing the cities and towns mentioned in the text. The yellow star represents the epicenter of the 2015 Illapel Earthquake. The thin black lines are isobaths at water depths of 200, 1000 and 3000 m. The thick black line is the Peru-Chile trench.**

10

Figure 2: Photographs of structures undamaged and damaged by the 2015 tsunami in the Coquimbo area. The red letter d indicates the observed tsunami flow depth.

Figure 3. a) Surveyed damage to structures due to the 2015 tsunami. b) Coquimbo Inundated area (Aránguiz et al., 2016) and survey data.

5
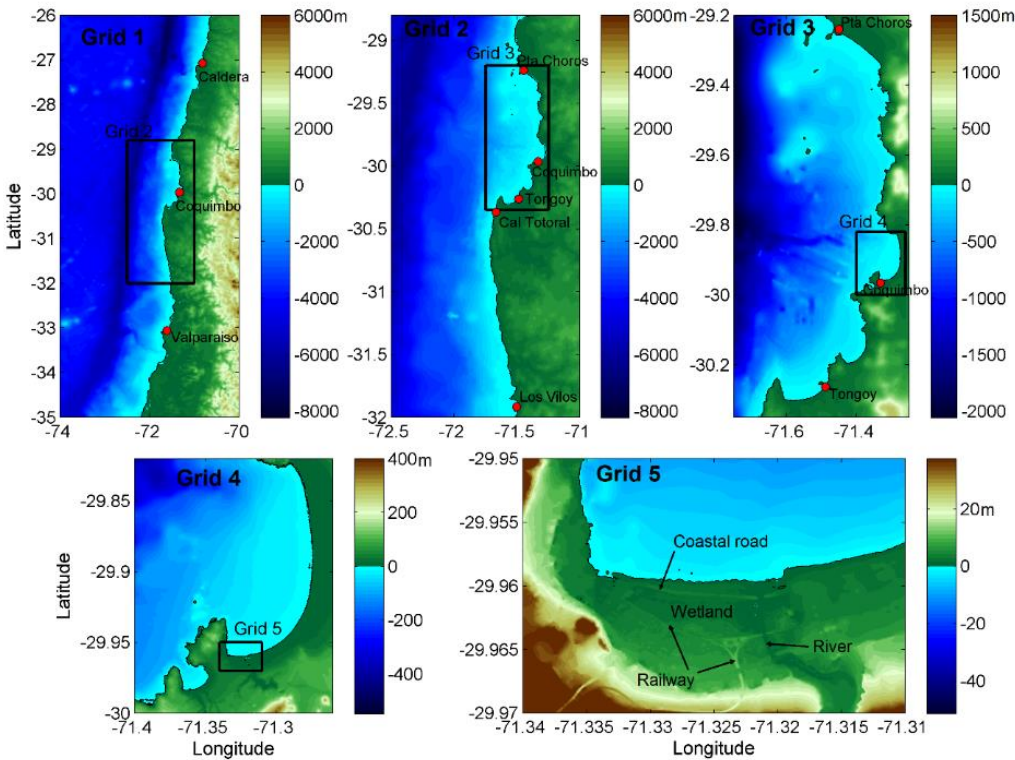
Figure 4. Model setting and nested computational grids for Coquimbo.

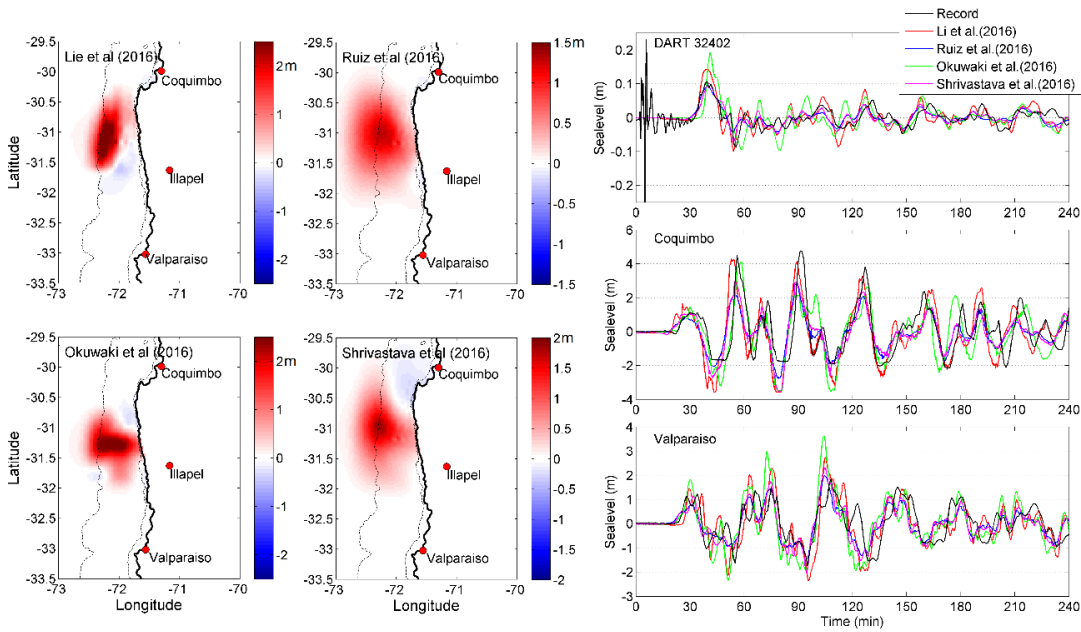Natural Hazards
and Earth System
Sciences
Discussions

Figure 5. Tsunami initial conditions of four source models and comparison of tsunami records with simulated tsunami waveforms at DART 32402, Coquimbo and Valparaiso.
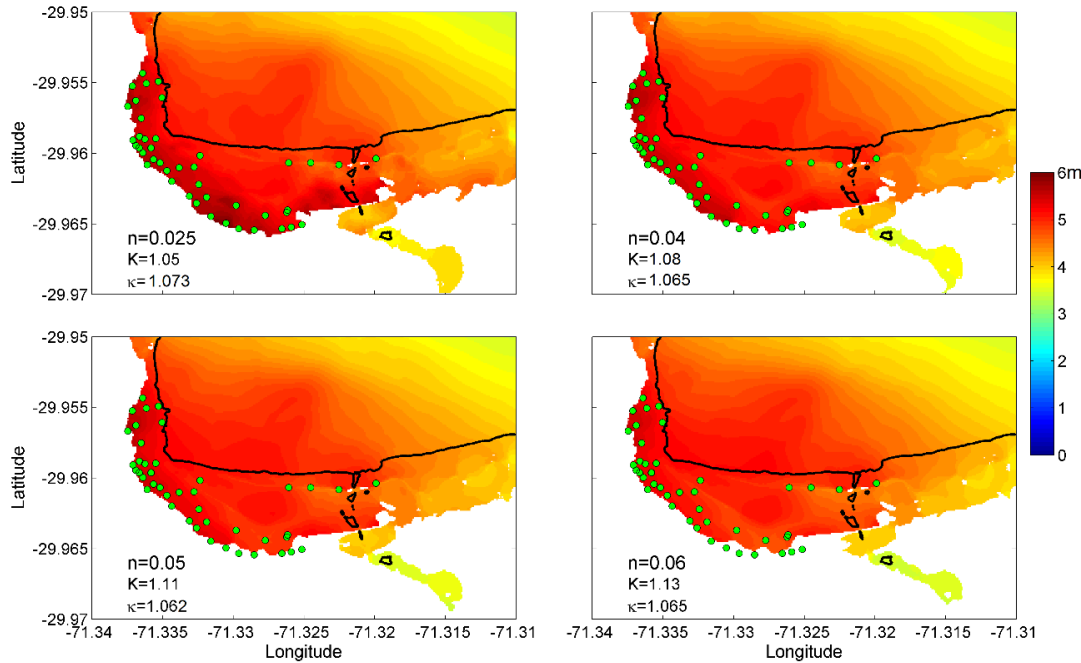

Figure 6. Tsunami inundation heights obtained with the modified Li et al. (2016) source model and four different Manning coefficients, n=0.025, 0.04, 0.05, 0.06. The parameters of root means square error, *K* and *κ* area also shown.
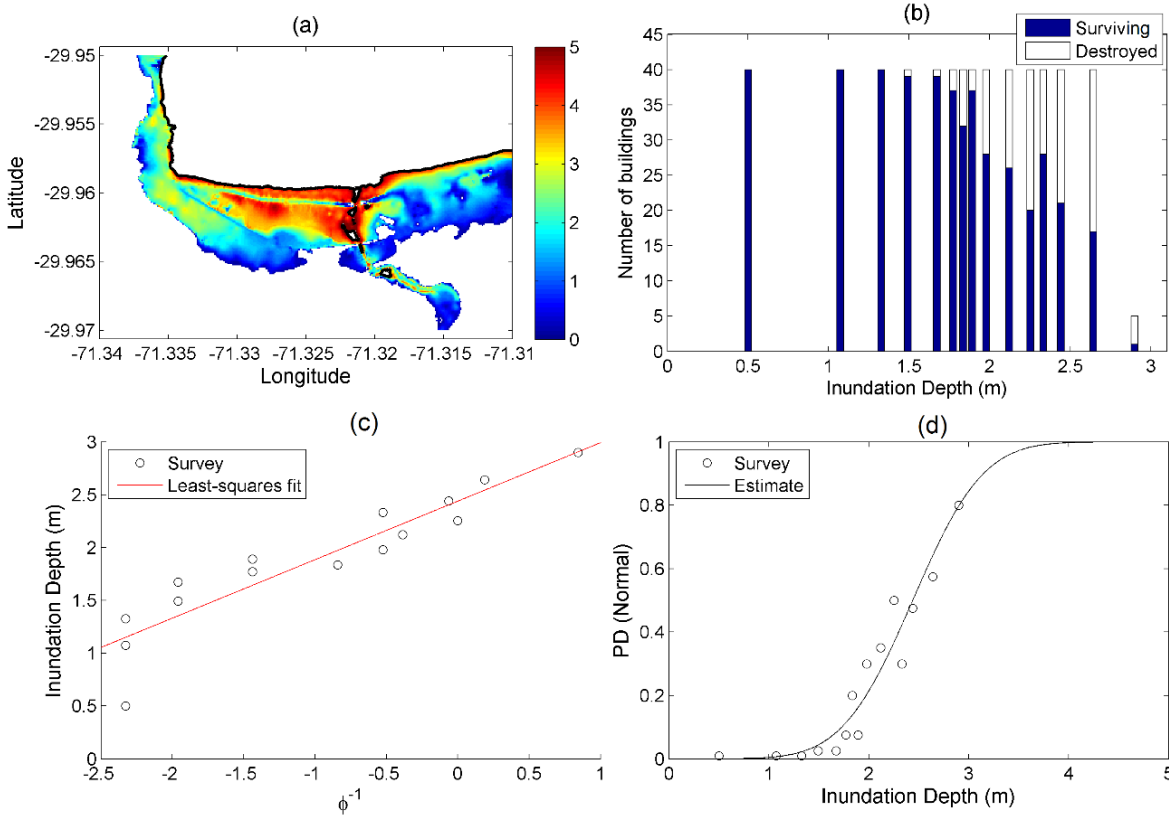
Figure 7. Developing the tsunami fragility curve. a) Inundation depths from Numerical simulation. b) Histogram of the number of destroyed and surviving structures in terms of the inundation depth within the inundation area. c) Plot on normal probability paper and least-squares fit. d) Fragility function for building damage in terms of inundation depth; the solid line is the best-fit curve of the plot (o: the distribution of damage probability).
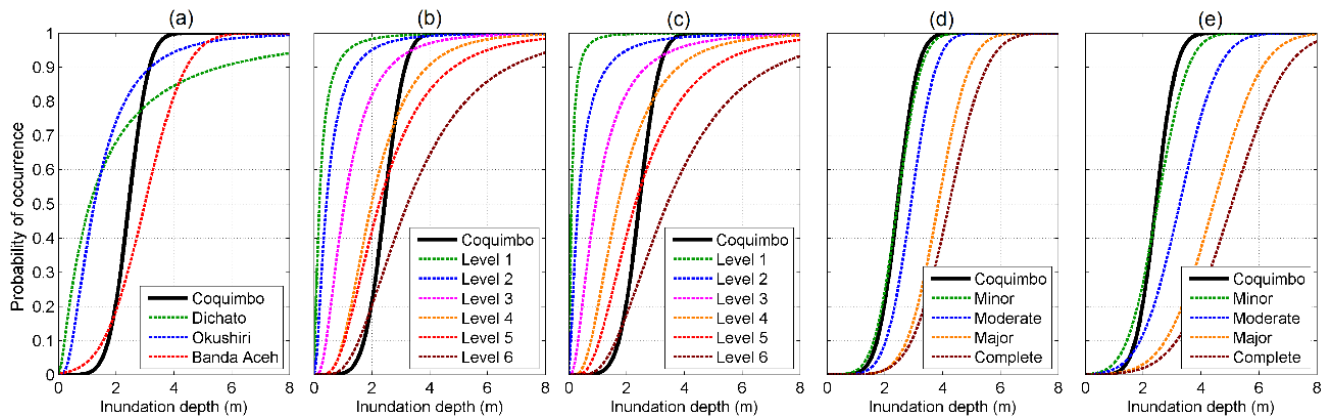

Figure 8. Tsunami fragility curves for damage probability developed for other locations and different damage levels. a) Two levels of damage obtained for three different cities in Chile, Japan and Indonesia. b) Six damage levels for wooden structures given by Suppasri et al., (2013). c) Six damage levels for mixed-material structures by Suppasri et al., (2013). d) Four damage levels for wooden houses given by Suppasri et al., (2012). e) Four damage levels for mixed-material structures given by Suppasri et al., (2012).
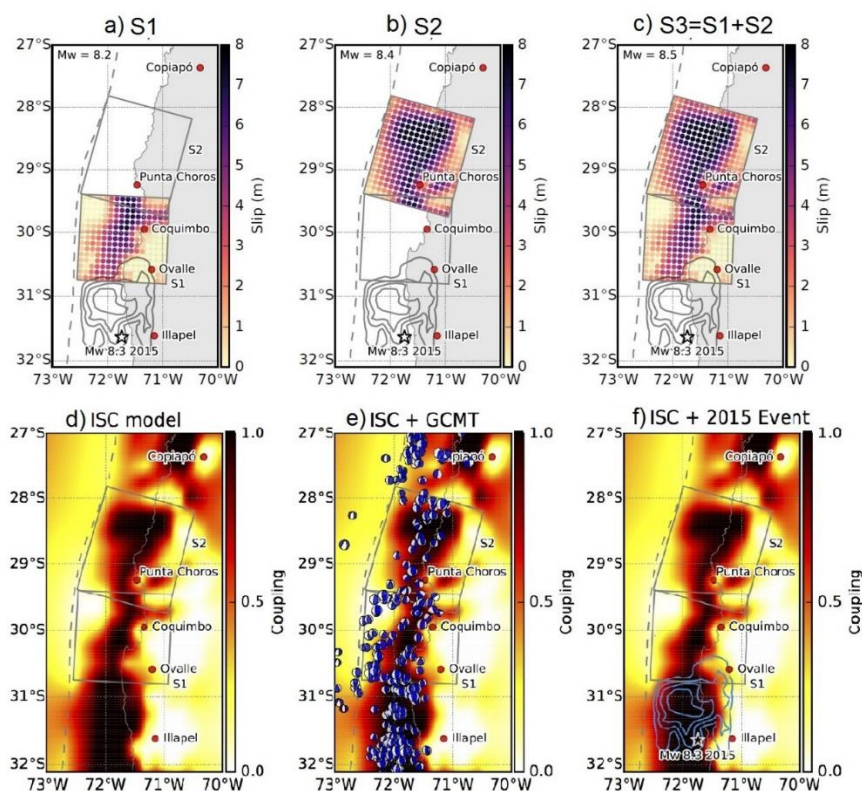
Figure 9. Upper panel: Slip distributions along scenario source models. The gray rectangles outline each scenario source segment. The moment magnitude for each scenario source model is denoted in the left-top of the corresponding panel. Lower panel: (left) the ISC model from the Métois et al., (2016), (center) GCMT solutions, and (right) the inverted slip model from Okuwaki et al., (2016), which are considered for construction of scenario source models. The star denotes the epicenter of the 2015 Illapel earthquake determined by the Centro Sismológico Nacional (CSN). The blue contours delimit the inverted slip distribution every 2.08 m for the 2015 Illapel earthquake (Okuwaki et al., 2016)
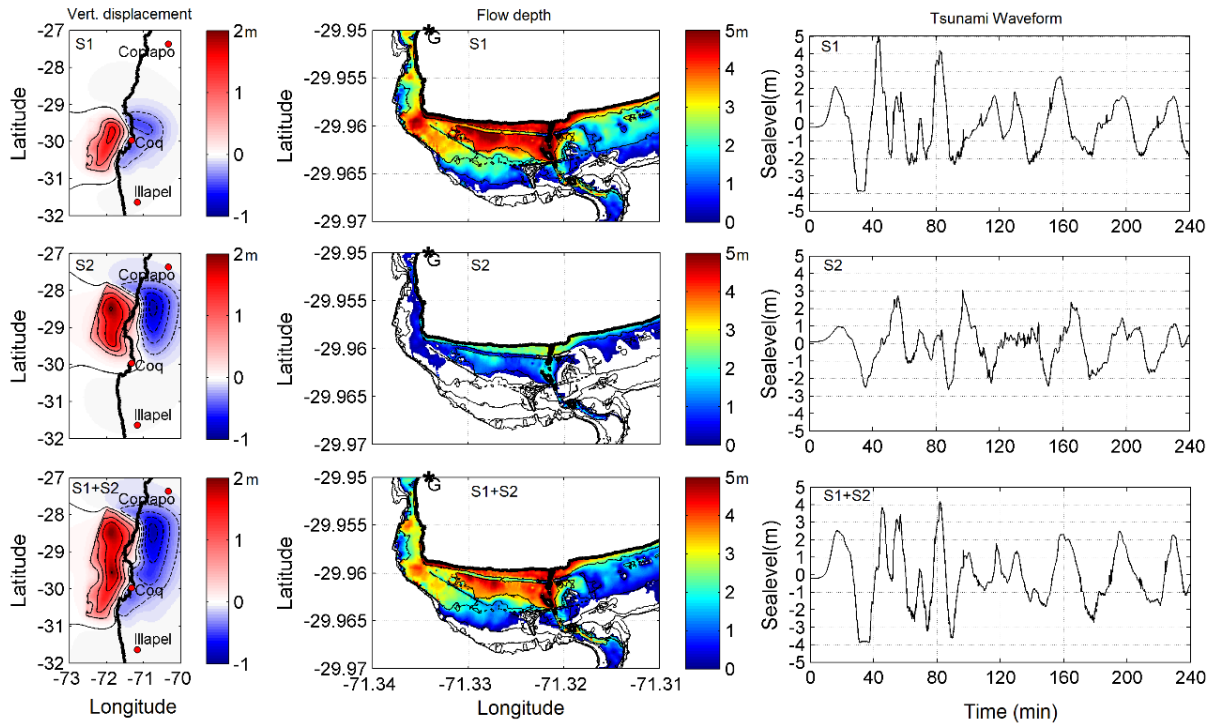
Figure 10. Results of tsunami numerical simulations for case 1 and the three scenarios, S1, S2 and S1+S2. Left row: vertical seafloor displacement. Central row: maximum inundation depth; the asterisk indicates the location of the tide gauge. Right row: tsunami wave form during an elapsed time of 4 h at the Coquimbo tide gauge G.
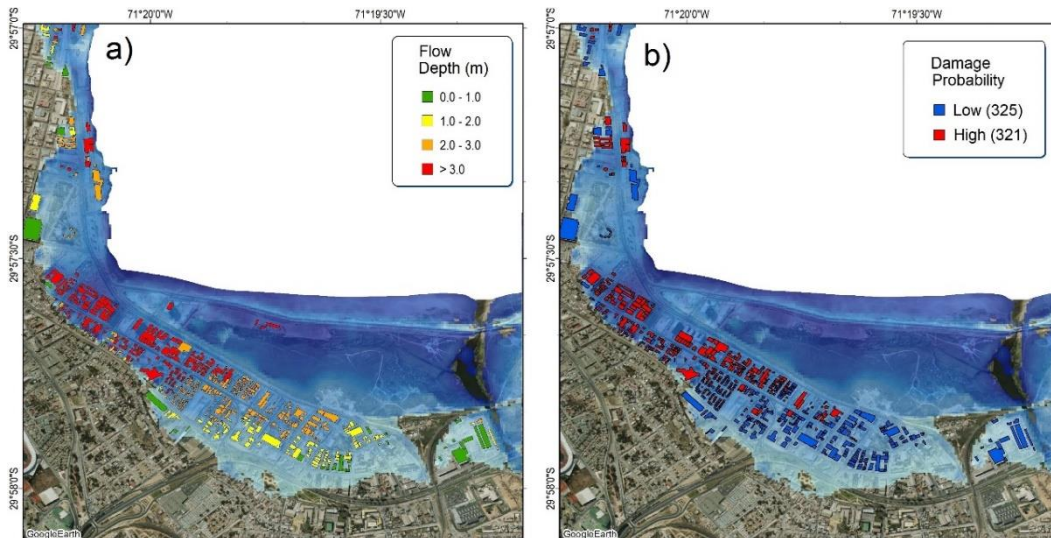

Figure 11. a) Tsunami inundation map and flow depth on structures. b) Tsunami inundation map and low and high probabilities of damage to the flooded structures.